

LETTER

Gate tunable magneto-resistance of ultra-thin WTe₂ devices

To cite this article: Xin Liu *et al* 2017 *2D Mater.* **4** 021018

View the [article online](#) for updates and enhancements.

Related content

- [Effect of aging-induced disorder on the quantum transport properties of few-layer WTe₂](#)
Wei Lai Liu, Mao Lin Chen, Xiao Xi Li et al.
- [Magnetoresistance and Hall resistivity of semimetal WTe₂ ultrathin flakes](#)
Xin Luo, Chi Fang, Caihua Wan et al.
- [Few-layer 1T MoTe₂ as gapless semimetal with thickness dependent carrier transport](#)
Peng Song, Chuanghan Hsu, Meng Zhao et al.



IOP | ebooks™

Bringing you innovative digital publishing with leading voices to create your essential collection of books in STEM research.

Start exploring the collection - download the first chapter of every title for free.

2D Materials



LETTER

Gate tunable magneto-resistance of ultra-thin WTe₂ devices

RECEIVED
17 January 2017

REVISED
12 February 2017

ACCEPTED FOR PUBLICATION
17 February 2017

PUBLISHED
8 March 2017

Xin Liu¹, Zhiran Zhang¹, Chaoyi Cai¹, Shibing Tian¹, Satya Kushwaha², Hong Lu¹, Takashi Taniguchi³, Kenji Watanabe³, Robert J Cava², Shuang Jia^{1,4} and Jian-Hao Chen^{1,4}

¹ International Center for Quantum Materials, Peking University, Beijing 100871, People's Republic of China

² Department of Chemistry, Princeton University, Princeton, NJ, United States of America

³ High Pressure Group, National Institute for Materials Science, 1-1 Namiki, Tsukuba, Ibaraki 305-0044, Japan

⁴ Collaborative Innovation Center of Quantum Matter, Beijing 100871, People's Republic of China

E-mail: liux23@pku.edu.cn (X Liu), jiashuang@gmail.com (S Jia) and chenjianhao@pku.edu.cn (J-H Chen)

Keywords: transition metal dichalcogenide, electronic device, solid-dielectric gate, magneto-resistance

Supplementary material for this article is available [online](#)

Abstract

In this work, the magneto-resistance (MR) of ultra-thin WTe₂/BN heterostructures far away from electron–hole equilibrium is measured. The change of MR of such devices is found to be determined largely by a single tunable parameter, i.e. the amount of imbalance between electrons and holes. We also found that the magnetoresistive behavior of ultra-thin WTe₂ devices is well-captured by a two-fluid model. According to the model, the change of MR could be as large as 400 000%, the largest potential change of MR among all materials known, if the ultra-thin samples are tuned to neutrality when preserving the mobility of 167 000 cm² V⁻¹ s⁻¹ observed in bulk samples. Our findings show the prospects of ultra-thin WTe₂ as a variable magnetoresistance material in future applications such as magnetic field sensors, information storage and extraction devices, and galvanic isolators. The results also provide important insight into the electronic structure and the origin of the large MR in ultra-thin WTe₂ samples.

Introduction

1T'-Tungsten ditelluride (WTe₂) is a layered transition metal dichalcogenide (TMDC) with a distorted structure that preserves inversion symmetry in the out-of-plan direction, contrasting with TMDCs with 2H phases, such as 2H-MoS₂ [1]. The material in its pristine bulk form is a semimetal [2, 3]. It exhibits rich physics such as extraordinarily large and non-saturating magneto-resistance (XMR) [4], superconductivity under high pressure [5, 6], and may be a type-II Weyl semimetal (WSM) at a particular level of electron doping [7–10]. Furthermore, reports on thin films of WTe₂ show the tunability of magnetoresistance revealing interesting new phenomena such as the transition from weak anti-localization to weak localization [11], the depletion of holelike carriers in the suppressed-MR regime [12], long-range field effect [13], the topological insulator-like behavior [14], and negative longitudinal MR indicating WTe₂ a type-II WSM [15]. The origin of the XMR in WTe₂, together with its potential application in magnetic field sensing and in information storage, has attracted much attention in the scientific and technical community [16–21]. The majority of the research in XMR has been

carried-out in bulk WTe₂ samples with near-perfect electron–hole compensation, and the results support the picture that the XMR arises from such near-perfect compensation of electrons and holes [17], i.e. a two-fluid picture. However, electrolyte gating experiments on thinner WTe₂ samples (~70 nm) have shown non-saturating XMR that deviates from the two-fluid theory [18]. Here, we have carried out careful experiments with solid-dielectric gated ultra-thin WTe₂ samples (~10 nm) that are far away from charge neutrality. We find that in this regime, the MR of the samples can still be well explained by the two-fluid model, and the sample shows 2D weak anti-localization effects at low temperatures. We also found that the change of MR of the ultra-thin WTe₂ is determined largely by the density difference between the electron and hole carriers, pointing to possible future application of this material in electric-field tunable, variable sensitivity magnetic field sensors [22–24].

Device fabrication and measurement

The ultra-thin WTe₂ samples measured in this letter are mechanically exfoliated from bulk WTe₂ crystal and transferred on to thin h-BN single crystals placed

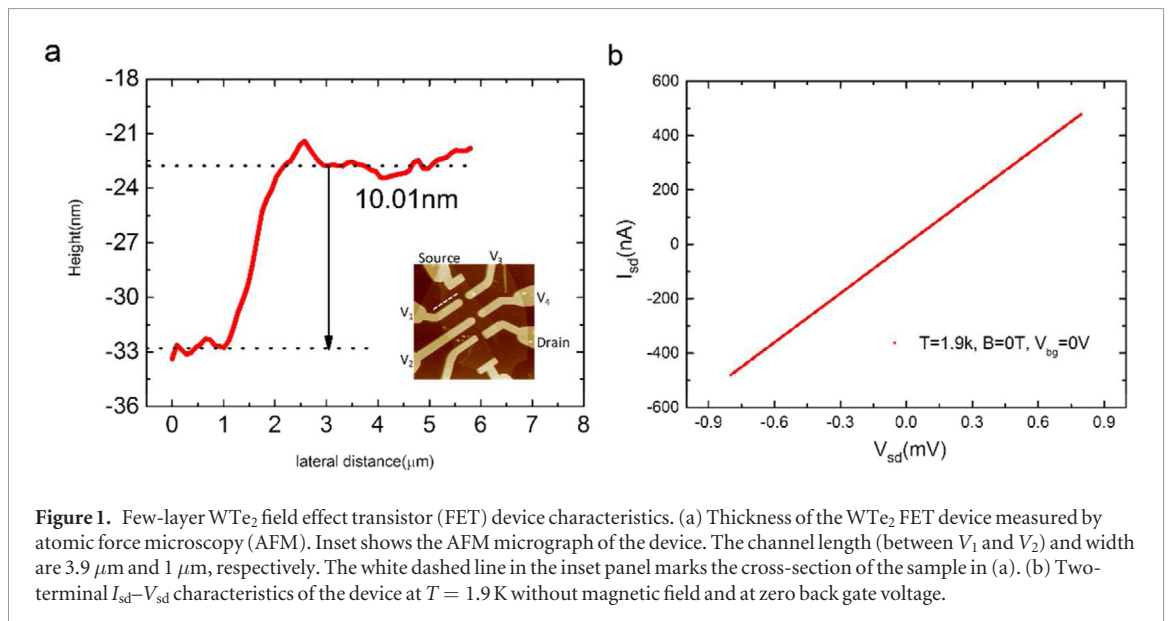


Figure 1. Few-layer WTe_2 field effect transistor (FET) device characteristics. (a) Thickness of the WTe_2 FET device measured by atomic force microscopy (AFM). Inset shows the AFM micrograph of the device. The channel length (between V_1 and V_2) and width are $3.9 \mu\text{m}$ and $1 \mu\text{m}$, respectively. The white dashed line in the inset panel marks the cross-section of the sample in (a). (b) Two-terminal $I_{\text{sd}}-V_{\text{sd}}$ characteristics of the device at $T = 1.9 \text{ K}$ without magnetic field and at zero back gate voltage.

on $300 \text{ nm SiO}_2/\text{Si}$ substrates [25]. We found that using single crystal BN substrates resulted in an increase in the mobility of our samples which are 10 nm thick or less (see section S4 at supporting information for details (stacks.iop.org/TDM/4/021018/mmedia)). WTe_2 bulk crystals are synthesized using chemical vapor transport technique [4] and h-BN bulk crystals are grown by the method described in [26]. The thin h-BN (thickness $\sim 15 \text{ nm}$) surface is free of dangling bonds, greatly alleviates the influence of surface charge traps in the SiO_2 layer, and could substantially improve quality of low-dimensional devices. Standard electron-beam lithography technique is used to pattern electrodes, consisting of 6 nm Cr and 60 nm Au , on the WTe_2 samples to form multi-terminal field effect devices (FEDs). We have taken particularly careful measures to ensure that the samples do not expose to ambient conditions at all. The sample preparation process, device fabrication process and electrical transport measurement are done in inert atmosphere, or with the sample capped with a protection layer. The protection layer consists of 200 nm thick polymethyl methacrylate (PMMA) or a bilayer of 200 nm PMMA and 200 nm MMA . Electrical- and magneto-transport measurements were carried out in a Quantum Design PPMS-9 with standard lock-in technique.

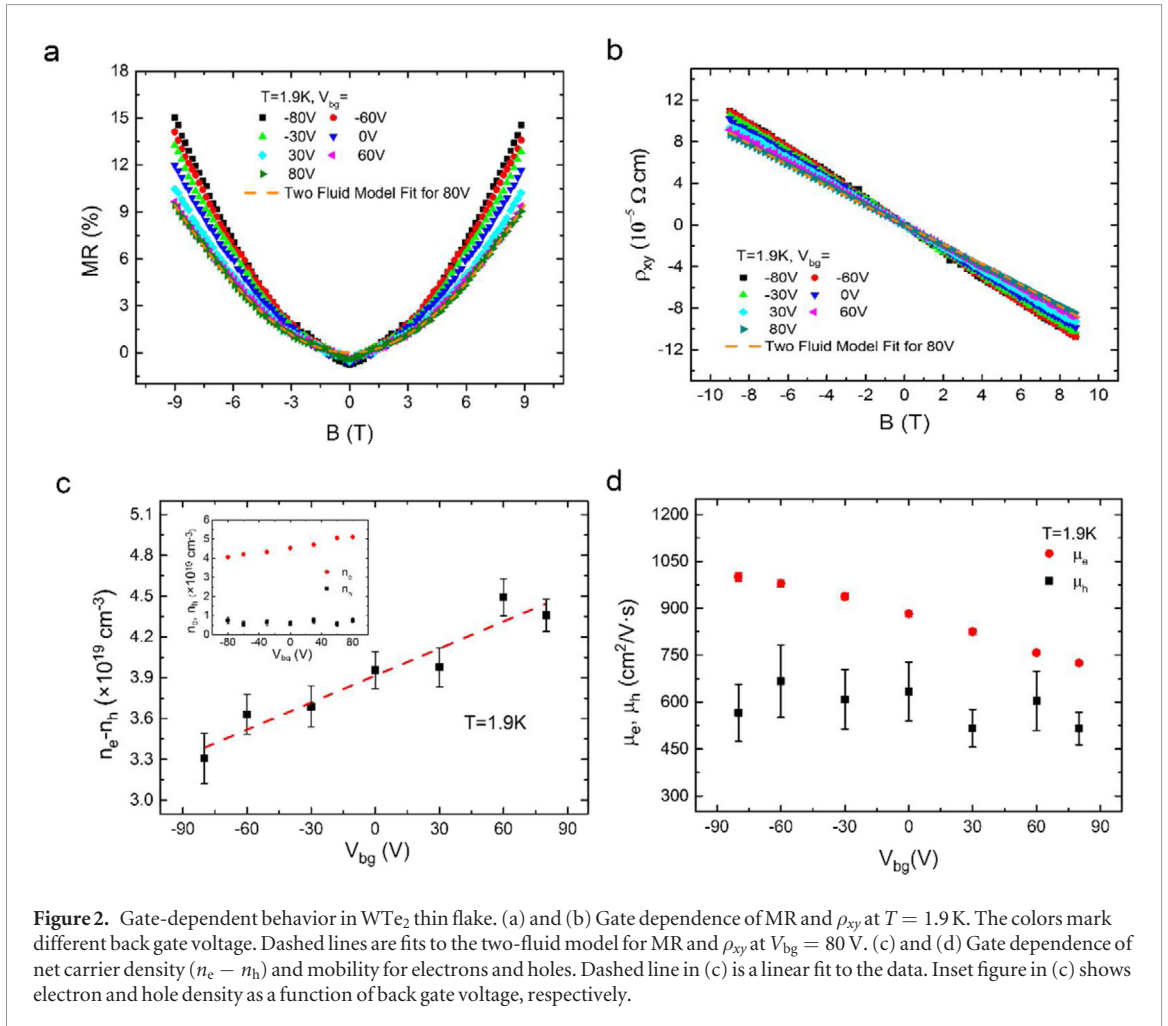
We shall focus our discussion on one device (sample A) in the main text; data for other WTe_2 devices are shown in supporting information. An atomic force microscopy (AFM) micrograph of a 10 nm -thick WTe_2 device as well as its height section profile is shown in figure 1(a). Figure 1(b) shows the $I-V$ characteristics of the WTe_2 FED at 1.9 K under zero magnetic field and zero back gate voltage, measured with two-probe configurations (between source and drain electrodes shown in the inset of figure 1(a)). The source-drain current (I_{sd}) varies quite linearly with the applied voltage V_{sd} from -0.8 mV to 0.8 mV , with resistivity of $4.26 \times 10^{-4} \Omega \cdot \text{cm}$, indicating an Ohmic contact to a metallic sample. Raman spectra of the device

(see section S3 in supporting information) obtained in a Horiba Jobin Yvon LabRam HR Evolution system after the transport experiments showed that the WTe_2 sample is indeed in the $1\text{T}'$ phase [27] and has not degraded.

Magneto-transport mechanism of WTe_2 FET devices

Figures 2(a) and (b) show the longitudinal magneto-resistance $\text{MR}(B) = (\rho_{xx}(B) - \rho_{xx}(B = 0))/\rho_{xx}(B = 0)$ and Hall resistance ρ_{xy} of the sample at $T = 1.9 \text{ K}$, with the magnetic field applied perpendicular to the sample surface (along the c axis), and at different back gate voltages. All measurements of magnetoresistance are done in four-probe configurations to eliminate contact effects. The sample exhibits a positive $\text{MR}(B)$ and quasi-linear $\rho_{xy}(B)$ under all the gate voltages investigated in this experiment. For small magnetic field, $\text{MR}(B)$ has a cusp-shape which will be discussed later. For magnetic fields larger than 1 T , $\text{MR}(B)$ can be fitted by a power law behavior, $\text{MR} \propto B^\gamma$, with the exponent γ between 1.62 and 1.69 for different gate voltages, which is smaller than the exponent $\gamma \sim 1.94$ observed in an 112 nm -thick sample (see section S1 in supporting information), and smaller than the exponent $\gamma \sim 2$ observed bulk crystals [4]. We will show later in this report that weak anti-localization should be taken into account (see figure 6) and the exponent γ is not a constant of magnetic field for electron-hole uncompensated samples (see section S7 in supporting information).

It has been found by transport [28–30] and ARPES [16, 17, 31, 32] experiments that bulk WTe_2 crystals have 4–9 carrier pockets; however, researchers are just starting to examine how these pockets evolve as the sample is getting thinner [33]. Here we started out to analyze the data with the ansatz that there are two major types of carriers in the sample, one type is electrons and the other type is holes. We will show that this ansatz captures the major-



ity of the physics in the high field magnetoresistance of ultra-thin WTe₂ samples, and that it is also consistent with low field magnetoresistance data.

In a two-fluid model [34], we have

$$\rho_{xx} = \frac{1}{e} \frac{(n_e u_e + n_h u_h) + (n_e u_h + n_h u_e) u_e u_h B^2}{(n_e u_e + n_h u_h)^2 + ((n_e - n_h) u_e u_h B)^2} \quad (1)$$

$$\rho_{xy} = \frac{1}{e} \frac{(n_e \mu_e^2 - n_h \mu_h^2) - (n_h - n_e) \mu_e^2 \mu_h^2 B^2}{(n_e u_e + n_h u_h)^2 + ((n_h - n_e) u_e u_h B)^2} \quad (2)$$

$$\begin{aligned} \text{MR} &= \frac{\rho_{xx}(B) - \rho_{xx}(B=0 \text{ T})}{\rho_{xx}(B=0 \text{ T})} \\ &= \frac{\frac{n_h}{n_e} (u_e + u_h)^2 u_e u_h B^2}{\left(u_e + \frac{n_h}{n_e} u_h\right)^2 + \frac{n_h}{n_e} \left(\left(\frac{n_h}{n_e} - 1\right) u_e u_h B\right)^2} \quad (3) \end{aligned}$$

where n_e (n_h) and u_e (u_h) are carrier density and mobility for electrons (holes), respectively. At all the gate voltages, both the MR and ρ_{xy} of the ultra-thin device can be simultaneously fitted by equations (2) and (3), and n_e , n_h , u_e , u_h can be extracted from the fit. Using the least squares method, we determine the values of the four parameters with minimum error (see section S9 in supporting information for details).

Figure 2(c) shows the net charge carrier density $n = n_e - n_h$ as a function of V_{bg} , and the dashed line is a linear fit to the data. The induced

charge in the sample by the silicon back gate is: $ne = C_g \Delta V_g$, where e is the elementary charge and C_g is the parallel-plate capacitance of the device per unit area. Thus from the linear fit, we obtained a gate capacitance of $C_g = 1.062 \times 10^{-4} \text{ F m}^{-2}$. Since the dielectric in our device consists of 15 nm of h-BN (relative permittivity $\epsilon_{\text{h-BN}} \approx 3.5$) and 300 nm of SiO₂ ($\epsilon_{\text{SiO}_2} \approx 3.9$), one can get the series capacitance for this multilayer system to

be $C'_g = \left(\frac{1}{C_{\text{h-BN}}} + \frac{1}{C_{\text{SiO}_2}}\right)^{-1} = 1.089 \times 10^{-4} \text{ F m}^{-2}$, in

good agreement with our experimental data. The above analysis show that the longitudinal magnetoresistance of the device can be tuned electrostatically and that the phenomenological two-fluid model captures the main feature of the magneto-transport properties of our ultra-thin WTe₂ samples. Note that the ultra-thin samples in this study are predominately electron-doped, with electron densities 5–10 times larger than hole densities; in comparison, thicker samples (the 112 nm-thick sample, see section S1 in supporting information) exfoliated from the same bulk crystal are found to be close to charge neutrality. The imbalance between electrons and holes in the ultra-thin devices are likely due to unintentional doping from the device fabrication process; such imbalance also allows us to access the highly electron-doped regime in ultra-thin WTe₂ samples to test the applicability of the two-fluid model [4, 18].

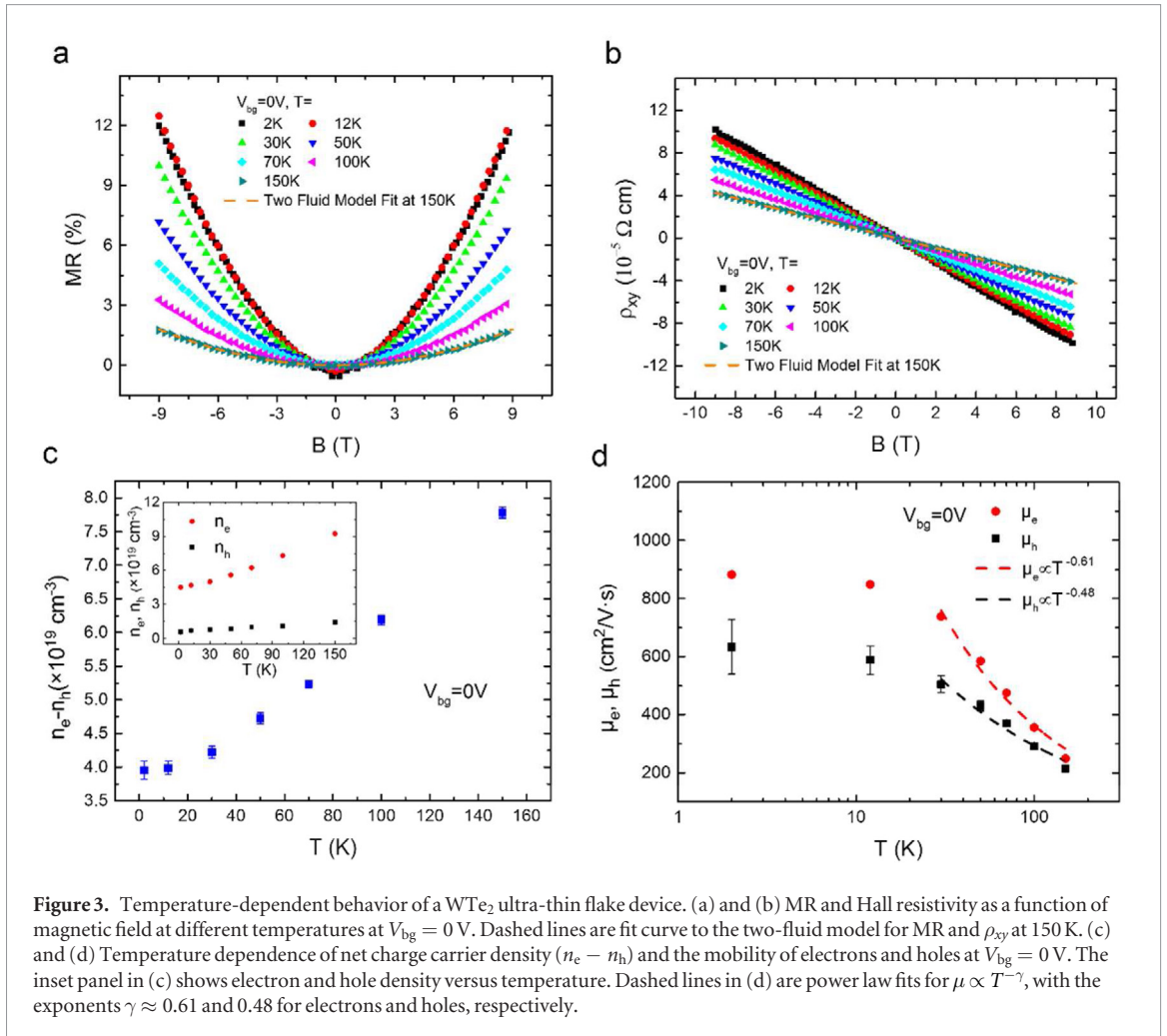


Figure 3. Temperature-dependent behavior of a WTe_2 ultra-thin flake device. (a) and (b) MR and Hall resistivity as a function of magnetic field at different temperatures at $V_{\text{bg}} = 0$ V. Dashed lines are fit curve to the two-fluid model for MR and ρ_{xy} at 150 K. (c) and (d) Temperature dependence of net charge carrier density ($n_e - n_h$) and the mobility of electrons and holes at $V_{\text{bg}} = 0$ V. The inset panel in (c) shows electron and hole density versus temperature. Dashed lines in (d) are power law fits for $\mu \propto T^{-\gamma}$, with the exponents $\gamma \approx 0.61$ and 0.48 for electrons and holes, respectively.

Figure 2(d) shows the gate-dependent mobility for electrons and holes. We note that the electron mobility decreases as the density becomes larger at $T = 1.9$ K, suggesting that charged impurities are not the dominating scattering source in this regime [35]. From figure 2(d) as well as from the inset of figure 2(c), we find that n_e and u_e are being effectively tuned by the gate voltage while n_h and u_h are much less affected by V_g , which is likely caused by the fact that the density of states of electrons is much larger than that of holes in this highly electron-doped regime.

Figures 3(a) and (b) show the temperature-dependent MR and ρ_{xy} of the device from $T = 1.9$ K to 150 K and at zero gate voltage. The cusp-shape in MR at small magnetic field diminishes rapidly as the temperature increases, and will be discussed in detail later. At magnetic field larger than 2 T, fitting the MR by a power law behavior $\text{MR} \propto B^\gamma$ results in a temperature-dependent exponent γ that changes from ~ 1.69 at $T = 1.9$ K to 2 at $T = 150$ K. At the meantime, ρ_{xy} remains linear in B with its slope k changes monotonically at different temperatures. We are going to show in this letter that such temperature-dependence of γ and k is also well captured by the phenomenological two-fluid model.

Similar to the analysis of the gate dependent magnetoresistance, the MR and ρ_{xy} of the device at different temperatures are fitted simultaneously by equations (2)

and (3), and the dependencies of n_e , n_h , u_e , u_h on temperature are extracted from the fit. Figure 3(c) shows the dependence of the net carrier charge $n_e - n_h$ as a function of temperature. It can be seen that by lowering the temperature, the sample rapidly tends to its charge neutrality on cooling from 150 K to 50 K; the trend slows down below 50 K and saturates from 12 K to 1.9 K. The mobilities u_e and u_h , on the other hand, increase following a power law of $\mu \propto T^{-\alpha}$ from 150 K to 50 K and then saturate from 12 K to 1.9 K. This suggests a connection between the decrease in $n_e - n_h$ and the increase of u_e and u_h , which is consistent with the carrier density dependent measurements at a fixed temperature. Temperature-dependent movement of chemical potential has been seen in multiple semimetal bulk crystals [31, 36–38], and has been attributed to be the cause of a temperature-induced Lifshitz transition for WTe_2 bulk crystals [31]. Thus it is not surprising to see such temperature-dependent $n_e - n_h$ in ultra-thin WTe_2 samples. A fit to a power law behavior of the decreasing mobility with increasing temperature give an exponent α for electrons ($\alpha = 0.61$) and holes ($\alpha = 0.48$); these values are similar to those for few-layer black phosphorus [39] and dual-gated monolayer MoS_2 [40]. However, they are smaller than the theoretically predicted value ($\alpha \sim 1.52$) [41] and smaller than our experimental data obtained from bulk WTe_2 samples ($\alpha \sim 1.30$ – 1.51)

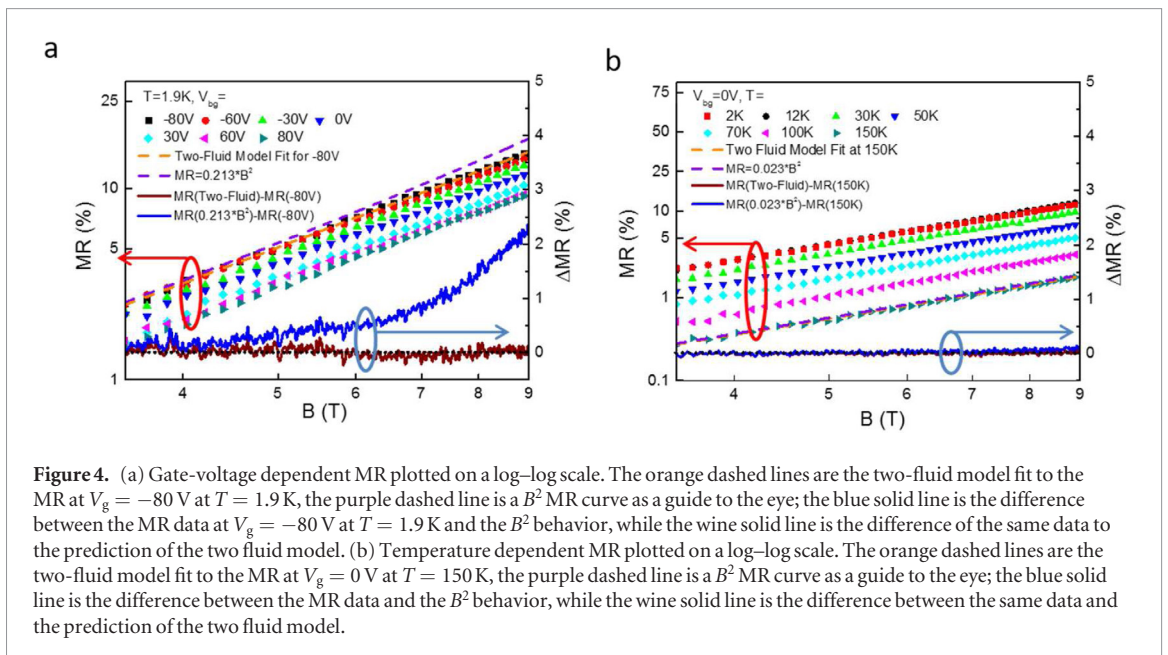


Figure 4. (a) Gate-voltage dependent MR plotted on a log–log scale. The orange dashed lines are the two-fluid model fit to the MR at $V_g = -80$ V at $T = 1.9$ K, the purple dashed line is a B^2 MR curve as a guide to the eye; the blue solid line is the difference between the MR data at $V_g = -80$ V at $T = 1.9$ K and the B^2 behavior, while the wine solid line is the difference of the same data to the prediction of the two fluid model. (b) Temperature dependent MR plotted on a log–log scale. The orange dashed lines are the two-fluid model fit to the MR at $V_g = 0$ V at $T = 150$ K, the purple dashed line is a B^2 MR curve as a guide to the eye; the blue solid line is the difference between the MR data and the B^2 behavior, while the wine solid line is the difference between the same data and the prediction of the two fluid model.

(see section S2 in supporting information). The suppression of α is considered to be caused by a quenching of the characteristic homopolar mode in sandwiched ultra-thin device structures [40]. In the case of WTe_2 , this means that ultra-thin samples can preserve their mobility, thus preserving their response to magnetic field, much better than their bulk counterparts at room temperature (see section S2 in supporting information), which is good for technological applications.

Since the ultra-thin WTe_2 sample is not at the charge neutral point, we expect a saturation of magnetoresistance for high enough magnetic field, if the transport behavior of the sample follows the two-fluid model. Indeed, if we look closely into the MR curves, we confirm such saturation at high magnetic field. Figures 4(a) and (b) show the gate-voltage dependent MR and temperature dependent MR plotted in log–log scale. It can be seen that for all the gate voltages we applied at 1.9 K, the MR of the sample deviates from the $\sim B^2$ functional form, while conforming to the prediction of the two-fluid model. In figure 4(a), the blue solid line is the difference between the MR data at $V_g = -80$ V at $T = 1.9$ K and the B^2 behavior, while the wine solid line is the difference of the same data to the prediction of the two fluid model. A deviation from the B^2 behavior (e.g. the saturation of MR at high magnetic field) is clearly observed. At higher temperature, the mobility of the carriers drops much faster than the increase in the net charge density of the sample, leading to a higher saturation magnetic field, which is out of the range of our experimental apparatus. Thus the MR data at 150 K fits the two-fluid model and a scaled B^2 functional form equally well (figure 4(b)).

Figure 5 is one of the primary observations of our study. It shows the change of MR as a function of $n_e - n_h$ at three different magnetic fields (7 T, 8 T, 9 T) and at all temperatures from 150 K to 1.9 K. (The change of MR is defined as $(MR(n) - MR(n_0))/MR(n_0)$, where $n = n_e - n_h$ is the net charge density

and $n_0 = 8.2 \times 10^{19} \text{ cm}^{-3}$ is the largest net charge density measured in our experiment, at $T = 150$ K.) It can be seen that the change of MR increases monotonically as $n_e - n_h$ decreases, regardless of temperature and magnetic field. The two-fluid model predicted $MR(n_e - n_h)$ curves for magnetic field of 7 T, 8 T and 9 T are also shown in figure 4, showing similar insensitivity to the magnetic field applied. This property of ultra-thin WTe_2 devices is very useful in making future tunable sensitivity magnetic field sensors, where a universal dependence on a single parameter (net charge carrier) is preferred. It is worth noting that such a curve is empirical, and it is a useful derivation from the two-fluid model. Experimentally, we found that for the carrier mobility about $1000 \text{ cm}^2 \text{ V}^{-1} \text{ s}^{-1}$ or lower, and for magnetic field 9 T or lower, such single-parameter dependence of ΔMR on $n_e - n_h$ holds pretty well.

The largest change of MR measured in our experiment is 850%, in which the 2D electron–hole imbalance is tuned from $8.2 \times 10^{19} \text{ cm}^{-3}$ to $3.2 \times 10^{19} \text{ cm}^{-3}$. If we reached charge neutrality in this particular device, the change of MR could be 8400% (see section S8 in supporting information for the calculation). Furthermore, as fabrication techniques improve, we expect the mobility of ultra-thin WTe_2 devices to finally approach that of bulk crystals. (Such rapid improvement of device fabrication techniques has been seen in the field of graphene, where it did not take a long time for the mobilities of graphene devices to improve from $10\,000 \text{ cm}^2 \text{ V}^{-1} \text{ s}^{-1}$ [42] to $100\,000 \text{ cm}^2 \text{ V}^{-1} \text{ s}^{-1}$ [25].) Using a fixed mobility value of $1.67 \times 10^5 \text{ cm}^2 \text{ V}^{-1} \text{ s}^{-1}$ from [43] for both $MR(p/n = 1)$ and $MR(p/n = 0.1559)$, we project a change of MR of 400 000%. Note that this should be a lower bound for the estimation, as the mobility at the neutrality point should be much higher than when $p/n = 0.1559$ (see figure 2(d) and supporting information for more details). Thus we expect ultra-thin WTe_2 to be a very useful electric-field-tuned magnetoresistance material in future technological applications.

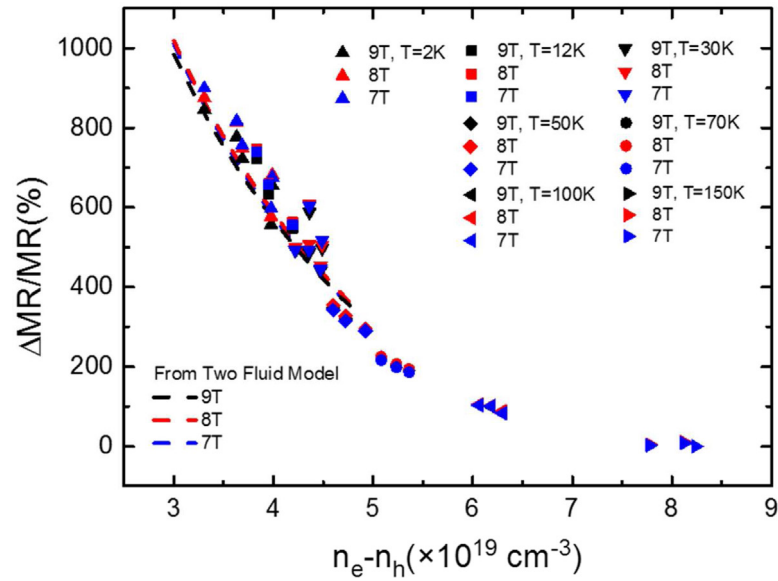


Figure 5. Tunable MR by carrier density in a WTe_2 ultra-thin flake device. Charge carrier density dependence of normalized MR, defined as $(\text{MR}(n) - \text{MR}(n_0))/\text{MR}(n_0)$, where $n = n_e - n_h$ is the net charge density and $n_0 = 8.2 \times 10^{19} \text{ cm}^{-3}$ is the largest net charge density measured in this device. Dashed lines are the two-fluid model prediction of $\text{MR}(n_e - n_h)$ curves for magnetic field of 7 T, 8 T and 9 T.

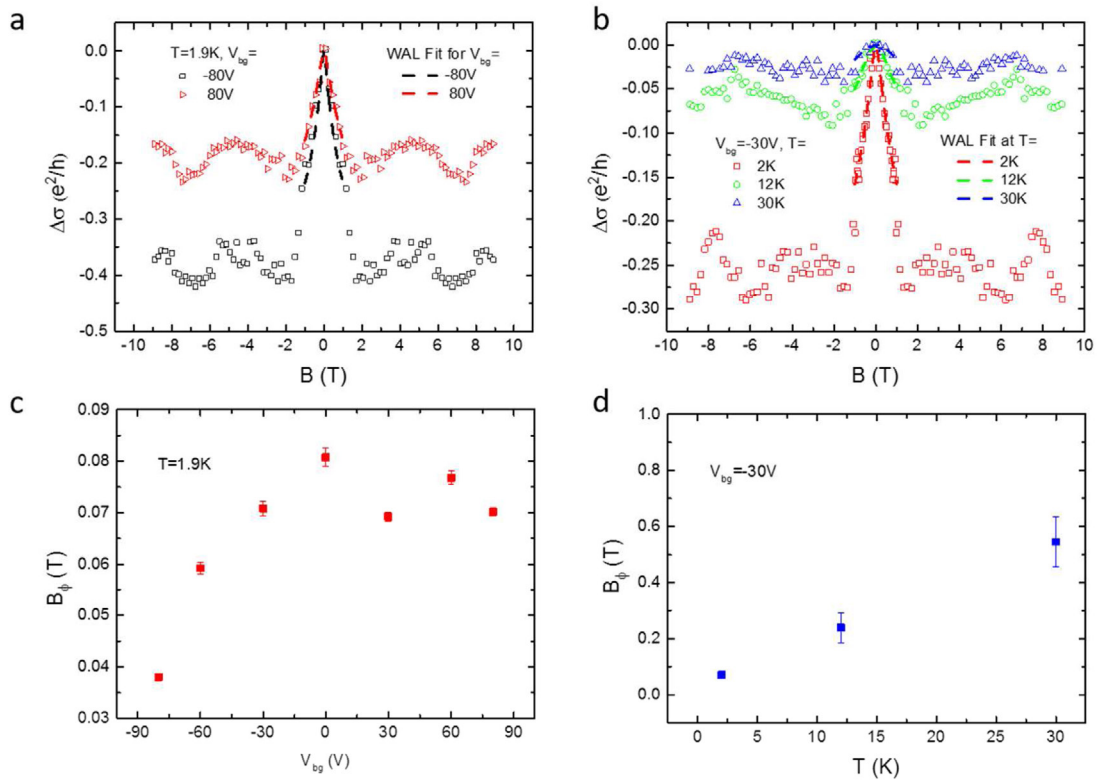


Figure 6. WAL in WTe_2 thin flake. (a) The change of conductance $\Delta\sigma_{xx}(B) = \sigma_{xx}(B) - \sigma_{xx}(B = 0)$ of the ultra-thin WTe_2 device at $T = 1.9 \text{ K}$ at largest gate voltages $V_g = \pm 80 \text{ V}$. (b) $\Delta\sigma_{xx}(B)$ curves for $T = 2 \text{ K}$, 12 K and 30 K at gate voltage $V_g = -30 \text{ V}$. The dashed lines in (a) and (b) are weak anti-localization fit to the data between $\pm 1 \text{ T}$ of magnetic field. (c) and (d) Phase related field B_ϕ as a function of back gate voltage at $T = 1.9 \text{ K}$ (c) and at different temperatures at $V_g = -30 \text{ V}$ (d).

Continuing the analysis of our observations, figure 6(a) shows the change of conductance $\Delta\sigma_{xx}(B) = \sigma_{xx}(B) - \sigma_{xx}(B = 0)$ of the ultra-thin WTe_2 device at $T = 1.9 \text{ K}$, after subtracting the classical contribution determined by the two-fluid model, and for the largest gate voltages ($V_g = \pm 80 \text{ V}$) applied

in experiment. The low field magneto-conductance shows a peak that can be strongly modified by the gate voltage. Figure 6(b) shows the $\Delta\sigma_{xx}(B)$ curves for $T = 2 \text{ K}$, 12 K and 30 K , with $V_g = 30 \text{ V}$. It can be seen that the low field magneto-conductance diminishes rapidly as T increases. Above 30 K , the peak in low field

magneto-conductance can no longer be detected. The magnitude and the temperature dependence of the low field magneto-conductance are characteristics of 2D weak anti-localization, similar to previously reported result in ultra-thin WTe_2 devices [15, 19]. We fit our experimental data to the Hikami–Larkin–Nagaoka (HLN) equation [44]:

$$\begin{aligned} \Delta\sigma_{xx}(B) = & -\frac{e^2}{2\pi^2\hbar} \left[\psi\left(\frac{1}{2} + \frac{B_\phi}{B}\right) - \ln\left(\frac{B_\phi}{B}\right) \right. \\ & - 2\psi\left(\frac{1}{2} + \frac{B_\phi + B_{so}}{B}\right) + 2\ln\left(\frac{B_\phi + B_{so}}{B}\right) \\ & \left. - \psi\left(\frac{1}{2} + \frac{B_\phi + 2B_{so}}{B}\right) + \ln\left(\frac{B_\phi + 2B_{so}}{B}\right) \right] \quad (4) \end{aligned}$$

where ψ is the digamma function, $B_n = \frac{\hbar}{4eD\tau_n} = \frac{\hbar}{4eD\tau_n}$, $n = \phi$, so is the characteristic field related to phase coherence length (time) l_ϕ (τ_ϕ) and spin–orbit interaction terms. D is the diffusion constant. In small magnetic field ($B < 1$ T), we find B_{so} is too large to affect $\Delta\sigma_{xx}(B)$. Hence, following the literature, we fitted $\Delta\sigma_{xx}(B)$ curves by setting $B_{so} = 6$ T [19]. Figure 6(c) shows the dependence of the fitting parameter B_ϕ on V_g at $T = 1.9$ K. It can be seen that B_ϕ drops by 50% if V_g changes from 80 V to -80 V, indicating a significant increase in the phase coherence length of charge carriers as the sample tends to charge neutrality, consistent with the magnetoresistance data at higher magnetic field. B_ϕ increases linearly with temperature, which could be a manifestation of strong electron–electron interaction in the material [19, 45, 46].

Conclusion

In summary, we have fabricated ultra-thin WTe_2 FEDs with solid gate dielectrics, and found that in electron-dominated regime, ultra-thin WTe_2 samples have a gate tunable magnetoresistance that is consistent with the two-fluid model. We estimate that the value of $\Delta\text{MR}/\text{MR}$ could be as high as 400 000% within experimentally accessible parameters, a value much higher than other materials. The tunability of MR by a single parameter (the net charge density $n = n_e - n_h$) together with the insensitivity of $\Delta\text{MR}/\text{MR}$ to magnetic field and temperature, reveal the potential of ultra-thin WTe_2 as electric-field-tuned magnetoresistance material which could have important application in magnetic field sensing, information storage and extraction, and galvanic isolation.

Acknowledgment

This project has been supported by the National Basic Research Program of China (973 Grant Nos. 2013CB921900, 2014CB920900), and the National Natural Science Foundation of China (NSFC Grant Nos. 11374021) (X Liu, Z Zhang, C Cai, S Tian,

J-H Chen). KW and TT acknowledge support from the Elemental Strategy Initiative conducted by the MEXT, Japan and a Grant-in-Aid for Scientific Research on Innovative Areas ‘Science of Atomic Layers’ from JSPS. The work at Princeton University was supported by the ARO MURI on topological insulators, grant W911NF-12-1-0461. We are grateful to Professor Alberto Morpurgo for inspiring discussions.

Author contributions

XL and JC conceived the experiment. XL exfoliated the WTe_2 thin flakes and few-layer h-BN crystals and accomplished the fabrication of the heterojunction FET devices. SK, HL, SJ and RJC grew WTe_2 bulk crystals; TT and KW grew h-BN bulk crystals. XL, ZZ, CC and ST performed the transport measurements and Raman measurements. XL, CC, ZZ and JC discussed the results and analyzed the data. XL and JC wrote the manuscript and all authors commented on it.

References

- [1] Mattheiss L F 1973 Band structures of transition-metal-dichalcogenide layer compounds *Phys. Rev. B* **8** 3719–40
- [2] Kabashima S 1966 Electrical properties of tungsten-ditelluride WTe_2 *J. Phys. Soc. Japan* **21** 945
- [3] Augustin J, Eyert V, Böker T, Frentrup W, Dwelk H, Janowitz C and Manzke R 2000 Electronic band structure of the layered compound Td- WTe_2 *Phys. Rev. B* **62** 10812
- [4] Ali M N *et al* 2014 Large, non-saturating magnetoresistance in WTe_2 *Nature* **514** 205
- [5] Pan X-C *et al* 2015 Pressure-driven dome-shaped superconductivity and electronic structural evolution in tungsten ditelluride *Nat. Commun.* **6** 7805
- [6] Kang D *et al* 2015 Superconductivity emerging from a suppressed large magnetoresistant state in tungsten ditelluride *Nat. Commun.* **6** 7804
- [7] Soluyanov A A, Gresch D, Wang Z, Wu Q, Troyer M, Dai X and Bernevig B A 2015 Type-II Weyl semimetals *Nature* **527** 495–8
- [8] Wu Y, Mou D, Jo N H, Sun K, Huang L, Bud’ko S L, Canfield P C and Kaminski A 2016 Observation of Fermi arcs in the type-II Weyl semimetal candidate WTe_2 *Phys. Rev. B* **94** 121113
- [9] Bruno F Y *et al* 2016 Observation of large topologically trivial Fermi arcs in the candidate type-II Weyl semimetal WTe_2 *Phys. Rev. B* **94** 121112
- [10] Wang C *et al* 2016 Observation of Fermi arc and its connection with bulk states in the candidate type-II Weyl semimetal WTe_2 *Phys. Rev. B* **94** 241119
- [11] Zhang E *et al* 2017 Tunable positive to negative magnetoresistance in atomically thin WTe_2 *Nano Lett.* **17** 878
- [12] Fatemi V, Gibson Q D, Watanabe K, Taniguchi T, Cava R J and Jarillo-Herrero P 2017 Magnetoresistance and quantum oscillations of an electrostatically tuned semimetal-to-metal transition in ultrathin WTe_2 *Phys. Rev. B* **95** 041410
- [13] Wang L, Gutiérrez-Lezama I, Barreteau C, Ki D-K, Giannini E and Morpurgo A F 2016 Direct observation of a long-range field effect from gate tuning of nonlocal conductivity *Phys. Rev. Lett.* **117** 176601
- [14] Fei Z, Palomaki T, Wu S, Zhao W, Cai X, Sun B, Nguyen P, Finney J, Xu X and Cobden D H 2016 Topological insulator behavior in monolayer WTe_2 (arXiv:1610.07924)
- [15] Wang Y *et al* 2016 Gate-tunable negative longitudinal magnetoresistance in the predicted type-II Weyl semimetal WTe_2 *Nat. Commun.* **7** 13142

- [16] Jiang J *et al* 2015 Signature of strong spin–orbital coupling in the large nonsaturating magnetoresistance material WTe_2 *Phys. Rev. Lett.* **115** 166601
- [17] Pletikoscic I, Ali M N, Fedorov A V, Cava R J and Valla T 2014 Electronic structure basis for the extraordinary magnetoresistance in WTe_2 *Phys. Rev. Lett.* **113** 216601
- [18] Wang Y, Wang K, Reutt-Robey J, Paglione J and Fuhrer M S 2016 Breakdown of compensation and persistence of nonsaturating magnetoresistance in gated WTe_2 thin flakes *Phys. Rev. B* **93** 121108
- [19] Wang L, Gutierrez-Lezama I, Barreteau C, Ubrig N, Giannini E and Morpurgo A F 2015 Tuning magnetotransport in a compensated semimetal at the atomic scale *Nat. Commun.* **6** 8892
- [20] Amin B, Kaloni T P and Schwingenschlogl U 2014 Strain engineering of WS_2 , WSe_2 , and WTe_2 *RSC Adv.* **4** 34561–5
- [21] Fei L, Jian W and Hong G 2015 Negative differential resistance in monolayer WTe_2 tunneling transistors *Nanotechnology* **26** 175201
- [22] Lenz J and Edelstein S 2006 Magnetic sensors and their applications *IEEE Sens. J.* **6** 631–49
- [23] Dang H B, Maloof A C and Romalis M V 2010 Ultrahigh sensitivity magnetic field and magnetization measurements with an atomic magnetometer *Appl. Phys. Lett.* **97** 151110
- [24] Chen Y, Gillette S M, Fitchorov T, Jiang L, Hao H, Li J, Gao X, Geiler A, Vittoria C and Harris V G 2011 Quasi-one-dimensional miniature multiferroic magnetic field sensor with high sensitivity at zero bias field *Appl. Phys. Lett.* **99** 042505
- [25] Wang L *et al* 2013 One-dimensional electrical contact to a two-dimensional material *Science* **342** 614–7
- [26] Taniguchi T and Watanabe K 2007 Synthesis of high-purity boron nitride single crystals under high pressure by using Ba–BN solvent *J. Cryst. Growth* **303** 525–9
- [27] Kong W-D, Wu S-F, Richard P, Lian C-S, Wang J-T, Yang C-L, Shi Y-G and Ding H 2015 Raman scattering investigation of large positive magnetoresistance material WTe_2 *Appl. Phys. Lett.* **106** 081906
- [28] Cai P L, Hu J, He L P, Pan J, Hong X C, Zhang Z, Zhang J, Wei J, Mao Z Q and Li S Y 2015 Drastic pressure effect on the extremely large magnetoresistance in WTe_2 : quantum oscillation study *Phys. Rev. Lett.* **115** 057202
- [29] Zhu Z, Lin X, Liu J, Fauqué B, Tao Q, Yang C, Shi Y and Behnia K 2015 Quantum oscillations, thermoelectric coefficients, and the Fermi surface of semimetallic WTe_2 *Phys. Rev. Lett.* **114** 176601
- [30] Xiang F-X, Veldhorst M, Dou S-X and Wang X-L 2015 Multiple Fermi pockets revealed by Shubnikov-de Haas oscillations in WTe_2 *Europhys. Lett.* **112** 37009
- [31] Wu Y, Jo N H, Ochi M, Huang L, Mou D, Bud'ko S L, Canfield P C, Trivedi N, Arita R and Kaminski A 2015 Temperature-induced Lifshitz transition in WTe_2 *Phys. Rev. Lett.* **115** 166602
- [32] Pan X-C *et al* 2016 Carrier balance and linear magnetoresistance in type-II Weyl semimetal WTe_2 *Front. Phys.* **12** 127203
- [33] Das P K *et al* 2016 Erratum: Layer-dependent quantum cooperation of electron and hole states in the anomalous semimetal WTe_2 *Nat. Commun.* **7** 11355
- [34] Hurd C M 1972 *The Hall Effect in Metals and Alloys* (Berlin: Springer)
- [35] Chen J-H, Jang C, Xiao S, Ishigami M and Fuhrer M S 2008 Intrinsic and extrinsic performance limits of graphene devices on SiO_2 *Nat. Nanotechnol.* **3** 206–9
- [36] Li Y, Wang Z, Lu Y, Yang X, Shen Z, Sheng F, Feng C, Zheng Y and Xu Z-A 2016 Negative magnetoresistance in topological semimetals of transition-metal dipnictides with nontrivial Z₂ Indices *Front. Phys.* **12** 127205
- [37] Wang Z, Li Y, Lu Y, Shen Z, Sheng F, Feng C, Zheng Y and Xu Z 2016 Topological phase transition induced extreme magnetoresistance in TaSb_2 (arXiv:1603.01717)
- [38] Zhang Y *et al* 2016 Electronic evidence of temperature-induced lifshitz transition and topological nature in ZrTe_5 (arXiv:1602.03576)
- [39] Li L, Yu Y, Ye G J, Ge Q, Ou X, Wu H, Feng D, Chen X H and Zhang Y 2014 Black phosphorus field-effect transistors *Nat. Nanotechnol.* **9** 372–7
- [40] Radisavljevic B and Kis A 2013 Mobility engineering and a metal–insulator transition in MoS_2 *Nat. Mater.* **12** 812
- [41] Kaasbjerg K, Thygesen K S and Jacobsen K W 2012 Phonon-limited mobility in n-type single-layer MoS_2 from first principles *Phys. Rev. B* **85** 115317
- [42] Zhang Y, Tan Y-W, Stormer H L and Kim P 2005 Experimental observation of the quantum Hall effect and Berry's phase in graphene *Nature* **438** 201–4
- [43] Mazhar N A, Leslie S, Jun X, Steven F, Quinn G, Max H, Ong N P and Cava R J 2015 Correlation of crystal quality and extreme magnetoresistance of WTe_2 *Europhys. Lett.* **110** 67002
- [44] Hikami S, Larkin A I and Nagaoka Y 1980 Spin–orbit interaction and magnetoresistance in the 2D system *Prog. Theor. Phys.* **63** 707
- [45] Neal A T, Liu H, Gu J and Ye P D 2013 Magneto-transport in MoS_2 : phase coherence, spin–orbit scattering, and the hall Factor *ACS Nano* **7** 7077
- [46] Hu J *et al* 2015 Enhanced electron coherence in atomically thin Nb_3SiTe_6 *Nat. Phys.* **11** 471–6